Positive-charged solid lipid nanoparticles as paclitaxel drug delivery system in glioblastoma treatment

Title: Positive-charged solid lipid nanoparticles as paclitaxel drug delivery system in glioblastoma treatment.

Author names and affiliations: Daniela Chirio[a], Marina Gallarate[a], Elena Peira[a], Luigi Battaglia[a], Elisabetta Muntoni[a], Chiara Riganti[b], Elena Biasibetti[c], Maria Teresa Capucchio[c], Alberto Valazza[c], Pierpaolo Panciani[d], Michele Lanotte[d], Laura Annovazzi[e], Valentina Caldera[e], Marta Mellai[e], Gaetano Filice[f], Silvia Corona[f], Davide Schiffer[e]

[a] University of Turin, Dipartimento di Scienza e Tecnologia del Farmaco, via Giuria 9, 10125 Torino, Italy.

daniela.chirio@unito.it, marina.gallarate@unito.it, elena.peira@unito.it, luigi.battaglia@unito.it, elisabetta.muntoni@unito.it

[b] University of Turin, Dipartimento di Oncologia, Regione Gonzole 10, 10043 Orbassano (TO), Italy.

chiara.riganti@unito.it

[c] University of Turin, Dipartimento di Scienze Veterinarie, Largo Paolo Braccini 2, 10095 Grugliasco (TO), Italy.

elena.biasibetti@unito.it, mariateresa.capucchio@unito.it, alberto.valazza@unito.it

[d] University of Turin, Dipartimento di Neuroscienze, Via Cherasco 15, 10126 Torino, Italy.

vincy.bip@alice.it, michele.lanotte@unito.it

[e] Policlinico di Monza, Centro di NeuroBioOncologia, Via Pietro Micca 29, 13100 Vercelli, Italy.

davide.schiffer@unito.it, laura.annovazzi@cnbo.it, valentina.caldera@cnbo.it, marta.mellai@cnbo.it

[f] IRCCS Policlinico San Matteo, University of Pavia, Dipartimento di Malattie Infettive, V.le Golgi 19, 27100 Pavia, Italy,

gaetano.filice@unipv.it

Corresponding Author: Daniela Chirio, via P. Giuria 9, 10125 Torino, Italy

daniela.chirio@unito.it

Phone: +39 0116707668 Fax: +39 0116707687

Abstract

Paclitaxel loaded solid lipid nanoparticles (SLN) of behenic acid were prepared with the coacervation technique. Generally, spherical shaped SLN with mean diameters in the range 300-600 nm were obtained. The introduction of charged molecules, such as stearylamine and glycol chitosan into the formulation allowed to obtain positive SLN with Zeta potential in the 8-20 mV range and encapsulation efficiency in the 25-90% range.

Blood-brain barrier (BBB) permeability, tested in vitro through hCMEC/D3 cells monolayer, showed a significantly increase in the permeation of Coumarin-6, used as model drug, when vehicled in SLN. Positive-charged SLN do not seem to enhance permeation although stearylamine-positive SLN resulted the best permeable formulation after 24 h.

Cytotoxicity studies on NO3 glioblastoma cell line demonstrated the maintenance of cytotoxic activity of all paclitaxel-loaded SLN that was always unmodified or greater compared with free drug. No difference in cytotoxicity was noted between neutral and charged SLN.

Co-culture experiments with hCMEC/D3 and different glioblastoma cells evidenced that, when delivered in SLN, paclitaxel increased its cytotoxicity towards glioblastoma cells.

Abbreviations:

PTX, paclitaxel; SLN, solid lipid nanoparticles; BA, behenic acid; ST, stearylamine; GCS, glycol chitosan; BBB, blood-brain barrier; GBM, blioblastoma multiforme; CNS, central nervous system; NP, nanoparticles; cationic bovine serum albumin, CBSA; NHEJ, non-homologous end joining; PK, protein Kinase; CS, chitosan; Cou-6, coumarin 6; Na-BA, sodium behenate; CHOL, cholesterol; FD, freeze-dried; DMEM, Dulbecco's modified Eagle's medium; NS, neurosphere;

AC, adherent cell; ATM, ataxia telangiectasia mutated; ChK2, checkpoint kinase; p-53BP1, 53 binding protein 1; MTT, 3-(4,5-dimethylthiazol-2-yl)-2,5diphenyl-tetrazolium bromide; IF, immunofluorescence; HR, homologous recombination; TEM, transmission electron microscopy; EE, entrapment efficiency; Pgp, P-glycoprotein; MRP1, multidrug resistance related protein 1.

Keywords: paclitaxel, SLN, coacervation, BBB permeability, cytotoxicity, glioblastoma

Chemical compounds studied in this article:

Paclitaxel (PubChem CID: 36314)

Coumarin-6 (PubChem CID: 100334)

Behenic acid (PubChem CID: 8215)

1. Introduction

Glioblastoma multiforme (GBM) is the most common form of primary brain tumor in the central nervous system (CNS); its aggressive nature and evasiveness to treatments make it one of the most lethal cancers [1]. Current treatments for GBM provide a tumor surgical resection followed by pharmacotherapy and radiotherapy. Pharmacotherapy, directed by residual tumor cells elimination, ranges from common chemotherapeutic agents such as temozolomide to more recent anti-angiogenic agents and immunotherapeutic treatments [2]. However, anti-cancer therapeutic agents have not significantly increased the median survival of GBM patients over the past 10 years. The 5-year survival rate of GBM patients after treatment that includes surgical resection, radiation and chemotherapy, is 9.8%.

The failure of chemotherapy is due to the inability of intravenously administered anticancer agents to reach the brain parenchyma. An endothelial cell monolayer associated with pericytes and astrocytes, known as the blood–brain barrier (BBB), separates blood from the cerebral parenchyma and prevents the penetration of drugs into the CNS.

BBB is a functional unit composed by the peculiar endothelium of brain microvessels, the capillary basal lamina and the surrounding astrocytes, neurons, microglial cells and pericytes, which contribute to the maintenance of the barrier properties [3, Figure A.1]. The presence of tight junctions and adherent junctions between adjacent endothelial cells [4], the lack of fenestrations and pinocytotic vesicles [5], the abundance of efflux transporters belonging to the ATP binding cassette family on the endothelium luminal side [6] account for the low delivery of drugs, such as antineoplastic agents [7], from the bloodstream to the brain parenchima.

Various invasive strategies have been developed to improve the penetration of drugs into the brain [8]. Traditional approach to overcome brain drug delivery obstacles includes direct intracerebral drug injection [9],which is associated with a high risk for the patient.

Less invasive strategies have also been investigated. One approach consists in generating a transient disruption of BBB in conjunction with the systemic administration of anticancer agents. The

intracarotid administration of a hyperosmotic solution such as mannitol led to a rapid diffusion of fluid across the cerebral endothelium, moving out of the endothelial cells into the vascular lumen and inducing the opening of the tight junctions for a few hours [10].

Another approach concerns the modification of drugs in order to make them more lipophilic, improving their penetration into the brain by passive diffusion. Lipophilic analogs and prodrugs were thus developed [11].

A more recent strategy to deliver drugs to the brain is the use of colloidal polymers to form nanometer sized carriers [12]. The basic reason of common acceptance of these vehicles is due to their drug release controlled profile of as well as to their selected targeting mechanism. Targeting action may be due to the steric hindrance created by nano-vectors: after parenteral administration, due to steric phenomenon they conceal themselves from opsonization event induced by tissue macrophages. By this way they achieve targeting ability to the brain and partially avoid other reticuloendothelial system organs like liver, spleen, etc [13].

From the last few decades, nanoparticles (NP) have attracted considerable interest in targeting drug molecules to the brain [14]. The correct mechanism of barrier opening by NP is not exactly known; the delivered NP enter into the brain by crossing the BBB by various endocytotic mechanisms, as polymeric albumin or poly(butylcyanoacrylate) NP are reported to enter into the brain by their small size mediated endocytosis [15,16]. An increased drug retention in brain blood capillaries combined with an adsorption to capillary can increase drug transport due to an enhanced concentration gradient; an increase of BBB fluidization, an opening of tight junctions between endothelial, an inhibition of the P-glycoprotein efflux system are other possible mechanisms that can increase brain drug concentration [17].

Although NP may be designed to entrap high molecular weight or hydrophilic therapeutics, BBB retardation of drug NP entrapped is based on NP characteristics and not on the therapeutic agent [18].

Indeed, poly(butyl cyanoacrylate) NP overcoated with 1% polysorbate 80 have been experimentally successful as brain drug delivery for doxorubicin [19] and dalargin [20], poly(lactic-co-glycolic acid) and cetyl alcohol/polysorbate NP for paclitaxel brain delivery [21,22].

In addition to BBB functional characteristics limiting permeation, brain microvasculature endothelia also present a luminal electrostatic barrier at physiologic pH. The negative electrostatic charge is created by surface expression and adhesion of the glycocalyx residues: proteoglycans, sulfated mucopolysaccharides, and sulfated and sialic acid-containing glycoproteins and glycolipids [23]. Cationic molecules have been shown to occupy anionic areas at the BBB endothelium [24] and increase BBB permeability via a presumed tight junction disruption [25].

Recent *in vitro* reports have demonstrated that positive-charged NP have an increased brain distribution compared to anionic and neutral NP [26]. However, there is little data regarding brain permeability of positive-charged NP. Lu et al. [27] developed and evaluated cationic bovine serum albumin (CBSA) conjugated with poly(ethyleneglycol)–poly(lactide) NP (CBSA–NP). To evaluate the effects of brain delivery, BSA conjugated with pegylated NP (BSA–NP) was used as the control group and Coumarin-6 was incorporated into the NP as the fluorescent probe. The qualitative and quantitative results of CBSA–NP uptake experiment compared with those of BSA–NP showed that rat brain capillary endothelial cells took in much more CBSA–NP than BSA–NP at 37 °C, at different concentrations and time incubations. After a dose of 60 mg/kg CBSA–NP or BSA–NP injection in mice caudal vein, fluorescent microscopy of brain coronal sections showed a higher accumulation of CBSA–NP in the lateral ventricle, third ventricle and periventricular region than that of BSA–NP. In an experimental work Lockman et al. [15] evaluated the effect of neutral, anionic and cationic charged NP on BBB integrity and NP brain permeability. Neutral NP and low concentrations of anionic NP had no effect on BBB integrity, whereas, high concentrations of anionic NP and cationic NP disrupted the BBB. The brain uptake rates of anionic NP at lower concentrations were higher than of neutral or cationic formulations at the same concentrations.

In literature, many authors studied solid lipid nanoparticles (SLN) as drug delivery systems to deliver drugs to the CNS [28,29]. SLN are disperse systems having size ranging from 1 to 1000 nm which represent an alternative to polymeric particulate carriers and are composed of physiological or biocompatible lipids or lipid molecules with a history of safe use in therapy and are generally suitable for intravenous administration.

As few data are present in literature about positive-charged SLN for brain delivery, the purpose of this work will be to prepare, characterize and evaluate in vitro the potential of positive-charged SLN to vehicle paclitaxel (PTX) to the brain for GBM treatment.

PTX, a diterpene isolated from *Taxus brevifolia*, is one of the most active chemotherapeutic agents against a wide panel of solid tumors including urothelial, breast, lung, and ovarian cancers. It has been demonstrated that PTX is effective against glioblastoma cells *in vitro* [30,31], however its clinical use is limited due to its poor BBB penetration capability and drug-resistance [32,33].

Due to its low water solubility, PTX is formulated in a mixture of Cremophor® EL and dehydrated ethanol (50:50 v/v) a combination known as Taxol®. However, Taxol® has some severe side effects related to Cremophor® EL and ethanol [34]. Therefore, there is an urgent need for the development of alternative PTX formulations.

Recently, a new solvent-free technique, defined as “coacervation”, was developed to prepare fatty acids-based SLN [35]. Briefly, a fatty acid alkaline salt micellar solution in the presence of an appropriate polymeric stabilizer was prepared; when the pH is lowered by acidification, the fatty acid precipitates as nanoparticles owing to proton exchange between the acid solution and the sodium salt.

SLN were prepared using two different positive-charged substances: ST or GCS. ST possess a hydrocarbonic chain that can probably be incorporated within the lipid matrix, while its positive charge is exposed to the external surface. GCS, a chitosan derivative conjugated with ethylene glycol branches, is a water soluble at a neutral/acidic pH values polymer whose pendant glycol branches increase both the aqueous solubility of the native chitosan (CS) and provide steric

166 stabilization [36]. Mao et al [37] have established that CS is capable of opening the tight junctions
167 of epithelial cells and it can improve the uptake of hydrophilic drugs including peptides.
168 For the above mentioned purpose, PTX loaded cationic SLN were prepared and extensively
169 characterized *in vitro* with regard to their physicochemical properties, their capacity to load and
170 release PTX, their cytotoxicity and their permeability across hCMEC/D3 cell lines taken as an *in*
171 *vitro* model of BBB.

2. Experimental

2.1 Chemicals

Sodium Behenate (Na-BA) was purchased from Nu-Chek Prep, Inc. (Elysian, U.S.A.), Tween®80, sodium dodecyl sulfate, Triton X-100 and cholesterol from Fluka (Buchs, Switzerland), paclitaxel (PTX) from Indena (Milan, Italy), citric acid from A.C.E.F. (Fiorenzuola d'Arda, Italy), 80% hydrolyzed PVA 9000–10000 Mw (PVA 9000), Pluronic F68, stearylamine (ST), glycol chitosan (GCS), coumarin 6 (Cou-6), triethanolamine phosphate, trehalose, penicilin-streptomycin, hydrocortisone, ascorbic acid, Hepes and b-FGF from Sigma (Dorset, UK), hydrochloric acid, sodium hydroxide and sodium phosphate monobasic from Merck (Darmstadt, Germany), Cremophor® EL from BASF (Ludwigshafen am Rhein, Germany), EBM-2 basal medium from Lonza, (Basel, Switzerland), fetal bovine serum Gold from PAA The Cell Culture Company (Pasching, Austria), rat collagen-I from Trevigen (Gaithersburg, Maryland, USA), chemically defined lipid concentrate from Invitrogen Life technologies (Carlsbad, California, USA), methanol and ethanol from Carlo Erba (Val De Reuil, France). Deionized water was obtained by a MilliQ system (Millipore, Bedford, MO).

2.2 hCMEC/D3 cells

hCMEC/D3 cells, a primary human brain microvascular endothelial cell line that retains the property of BBB *in vitro*, were cultured as reported [38]. Briefly, cells were maintained in Petri dishes coated with 150 µg/ml rat collagen-I and cultured in EBM-2 basal medium supplemented with 5% v/v fetal bovine serum Gold, 1% v/v penicilin-streptomycin, 1.4 µM hydrocortisone, 5 µg/ml ascorbic acid, 10 mM Hepes, 1% v/v Chemically Defined Lipid Concentrate, 1 ng/ml b-FGF. In all the experiments cells were used between passages 29 and 34. For the permeability assays, cells were seeded at 50,000/cm² and grown for 7 days up to confluence in Petri dishes and Transwell devices (0.4 µm diameter pores-size, Corning Life Sciences, Chorges, France), with 1.5

197 ml/cm^2 and 3 ml/cm^2 of the culture medium described above in the Transwell insert and in the
198 lower chamber, respectively.
199 Before each experiment we measured the transendothelial electrochemical resistance (TEER) and
200 the permeability coefficient of dextran-FITC, [^{14}C]-sucrose and [^{14}C]-inulin, taken as parameters
201 of paracellular transport across hCMEC/D3 monolayer, as described in [39]. TEER value was
202 between 30 and 40 Ω x cm^2, dextran-FITC permeability coefficient was 0.015 $\pm$ 0.003 x 10^{-3}
203 cm/min, [^{14}C]-sucrose permeability coefficient was 1.19 $\pm$ 0.21 x 10^{-3} cm/min, [^{14}C]-inulin
204 permeability coefficient was 0.56 $\pm$ 0.09 x 10^{-3} cm/min. These values suggested the functional
205 integrity of BBB monolayer [38].
206
207 *2.3 GBM cell lines and culture conditions*
208 Primary human GBM cell lines NO3 and CV17 were obtained from primary human GBMs
209 surgically resected at the Department of Neuroscience, Neurosurgical Unit, University of Turin,
210 Italy. The histological diagnosis was performed according to World Health Organization (WHO)
211 guidelines. The study was in compliance with the local institutional review board and Committee on
212 Human Research and with the ethical human-subject standards of the World Medical Association
213 Declaration of Helsinki Research. Written informed consent was obtained from all patients.
214 010627 GBM cell line was a kind gift of Dr. Galli R, DIBIT San Raffaele, Milan, Italy). For
215 cytotoxicity studies in co-culture models U87-MG cells (ATCC, Rockville, MD) were also used.
216 By neurosphere assay, from a resected tumor tissue we obtained neurosphere (NS) or adherent cell
217 (AC) or both cell types [40]. NS lines were cultured on Dulbecco's modified Eagle's medium
218 (DMEM)/F-12 supplemented with 20 ng/ml epidermal growth factor (EGF) and 10 ng/ml basic
219 fibroblast growth factor (bFGF); AC lines were grown on DMEM supplemented with 10% fetal
220 bovine serum (FBS) for AC. Both cultures were maintained at 37°C and at 5% O_2/CO_2 in a
221 humidified multigas Sanyo MCO-18M incubator (Sanyo Scientific, Bensenville, IL).

All cell cultures were periodically checked for *Mycoplasma* contamination (e-Myco^{TM} Mycoplasma PCR Detection kit, iNtRON Biotechnology, Korea).

2.4 PTX-loaded SLN preparation

Different SLN formulations were prepared (Table 1); non-charged SLN were prepared as reference to evaluate the positive-charge influence.

Non-charged SLN**:** SLN were prepared by the coacervation method [35]. Briefly, appropriate amounts of Na-BA and PVA 9000 were dispersed in 5 ml deionized water and the mixture was then heated under 5 min-stirring (300 rpm) just above the Krafft point of Na-BA (75 °C) to obtain a clear solution (micellar solution). A selected acidifying solution (100 µl 1M NaH_2PO_4 + 160 µl 1M HCl) was then added drop-wise until pH 4.0 was reached. The obtained BA SLN suspension was then cooled in a water bath under 10 min-stirring at 300 rpm until 15 °C temperature was reached. SLN suspension was then again heated under stirring (300 rpm) just above the melting point of BA (80 °C). Different amounts of 30 mg/ml ethanol PTX solution, heated at the same temperature of SLN suspension, were added to the warm mixture and then the sample was again cooled in a water bath under stirring at 300 rpm until 15 °C was reached.

Charged SLN**:** SLN were prepared as described for non-charged SLN, introducing the positive-charged agent as follows:

- ST-SLN**:** a fixed amount of 30 mg/ml 2-propanol ST solution (Table 1) was added to the warm aqueous Na-BA solution just above the Krafft point of Na-BA.
- GCS-SLN**:** an appropriate amount of GCS (Table 1) was added at the beginning of the preparation before obtaining the micellar solution.

All SLN formulations were also prepared in the presence of cholesterol (CHOL-SLN**)**: 100 or 150 µl of 5 mg/ml ethanol CHOL solution were added to the micellar solution immediately before the addition of the acidifying solution.

All SLN formulations were also prepared without drug (unloaded SLN) adding the same amount of ethanol instead PTX-ethanolic solution.

Fluorescent SLN to be employed in *in vitro* experiments were prepared using Cou-6 as fluorescent lipophilic model drug (Cou-6-CHOL-SLN). 5 ml SLN were prepared in aseptic conditions (under laminar flow airfilter starting from materials sterilized with UV or in autoclave) adding 100 µl 2mg/ml Cou-6 ethanol solution after SLN fusion. The samples were then cooled in a water bath under stirring at 300 rpm until 15°C temperature was reached.SLN were lyophilized using a programmable freeze-dryer (Shin PVTFD10R, Shinil Lab, Korea) without cryoprotectant addition. Slow freezing was carried out on the shelves in the freeze dryer (shelf temperature −40 °C). Samples were lyophilized for 24 h from −40 °C to 25 °C at a 5 °C/h. increasing rate. Lyophilized products were reconstituted by magnetic stirring adding the same water amount.

2.5 SLN characterization

SLN shape and mean sizes were characterized by Transmission electron microscope (TEM, CM 10 Philips, The Netherlands) spraying the SLN suspension on the microscope grid by means of an aerosol-sampling device.

Cou-6 localization into SLN dispersion was determined using optical microscopy equipped with a fluorescent lamp (Leica DM 2500, Solms, Germany) at 1000x magnification.

SLN particle sizes, polydispersity indexes (PDI) and Zeta potential were determined one hour after preparation using laser light scattering technique-LLS (Brookhaven, New York, USA). Size measurements were obtained at an angle of 90° at 25 °C using the number method. The dispersions were diluted with water for size determination or with 0.01 M KCl for Zeta-potential determination, in order to achieve the prescribed conductibility. Size measurements were also recorded diluting samples with grown medium used to culture hCMEC/D3 cells to mime the conditions under which SLN undergo in vitro experiments. For stability studies, the samples were stored at 4°C. All data were determined in triplicate.

PTX entrapment efficiency (EE%) was calculated as the ratio between PTX amount in SLN and that in the starting micellar solution × 100. PTX EE% determination was performed as follows: 1 ml SLN suspension was centrifuged for 15 min at 62,084 g, the precipitate was washed twice with 1 ml ethanol:water 30:70 to eliminate adsorbed PTX. The solid residue was dissolved in 1 ml ethanol, 0.5 ml water were then added to precipitate the lipid matrix and the supernatant obtained was injected in HPLC for PTX quantification.

EE% was also determined after 1:100 dilution in different media to mime the dilution that SLN can undergo after administration. Briefly, 500 µl SLN were introduced in a 50 ml flask and 49.5 ml water or 0.1 M phosphate buffer pH 7.4 or 0.1 M citric acid buffer pH 5.5 were added. The suspension was stirred for 2 hours. 8 ml suspension were centrifuged for 15 min at 62,084 g and then treated as previously described.

2.6 HPLC analysis

HPLC analysis was performed using a LC9 pump (Shimadzu, Tokyo, Japan) with a Chromosystem™ ODS 2.5 µ 125×4.6mm column and a C-R5A integrator (Shimadzu, Tokyo, Japan); mobile phase: CH_3CN:H_2O 60:40 (flow rate 1ml min^{-1}); detector: UV λ=227 nm (Shimadzu, Tokyo, Japan). Retention time was 2.6 min.

The limit of quantification, defined as the lowest PTX concentration in the curve that can be measured routinely with acceptable precision and accuracy, was 0.013 µmol/ml; the limit of determination, defined as the lowest detection limit, was 0.005 µmol/ml (signal to noise>2.0).

2.7 SLN and PTX stability

SLN sizes and PTX EE% of samples stored at 4 °C were monitored for 90 days to study SLN physical stability and PTX chemical stability. Mean sizes were determined by LLS and PTX EE% over time was obtained as described by HPLC.

298 The same SLN suspensions were freeze-dried without adding any cryoprotectant (FD-SLN) using a
299 Modulyo Freeze Dryer (Edwards Alto Vuoto, Italy). The resulting samples, rehydrated with the
300 same water amount, were also characterized by size, Zeta potential and EE% determination.
301
302 *2.8 PTX in vitro release*
303 *In vitro* release of PTX was determined using the non-equilibrium dialysis method [41]. A
304 multicompartmental rotating cell system consisting of donor and receptor compartments of equal
305 volume (1.5 ml) separated by a dialysis membrane (cut-off 12,000 Da) was used. Receiving
306 medium was 0.1 M phosphate buffer (pH 7.4) containing 0.1% v/v Tween®80. Solution of PTX in
307 receiving medium and SLN suspensions were used as donor formulations. At fixed times, the
308 receptor solution was tipped out and used for HPLC analysis and the cell was refilled with fresh
309 receiving medium. Drug concentration was determined by HPLC. The results were evaluated as
310 PTX apparent permeability constant (Kd_{app} [cm h^{-1}]) calculated from the slope of the straight line
311 obtained by plotting the amount of PTX diffused from the donor formulation versus time, assuming
312 pseudo zero-order kinetics.
313
314 *2.9 Permeability of SLN through hCMEC/D3 cell monolayer*
315 hCMEC/D3 cells, seeded as reported above in Transwell devices, were incubated at day 7 with
316 SLN 2, SLN 9, SLN 15 loaded with Cou-6, for 0.5, 3 and 24 h in the Transwell
317 insert. The amount of SLN added was 100 µl diluted with 900 µl of medium. This dilution of
318 SLN was the highest concentration devoid of cytotoxic effects on hCMEC/D3 cells, as previously
319 reported [42]. In parallel, a set of Transwell inserts were incubated with Cou-6 aqueous suspension
320 obtained with PVA 9000 as suspending agent, containing the same concentration of Cou-6
321 present in SLN. At the end of the incubation time, the medium in lower chamber was collected,
322 diluted 1: 20 into ethanol, sonicated with 10 bursts of 1 s to disrupt SLN, and centrifuged at 62,084
323 g for 5 min, to pellet debris. The dilution of the medium was necessary to obtain a fluorescence

falling in the detection range of the LS-5 spectrofluorimeter (PerkinElmer, Waltham, MA), used to measure the fluorescence of Cou-6.

Excitation and emission wavelengths were 485 ± 20 nm and 528 ± 20 nm, respectively. The fluorescence of Cou-6 at t_0 in the upper chamber, was considered 100%. The fluorescence of Cou-6 measured in the medium collected from the lower chamber was expressed as percentage of fluorescence in the upper chamber at t_0. The fluorescence of the medium without Cou-6 was considered as blank and was subtracted from the fluorescence of all the other experimental conditions.

To measure the amount of Cou-6 adsorbed on the Transwell membrane, Cou-6, either free or loaded in SLN, was added in empty Transwells in the same experimental conditions of the Transwells containing hCMEC/D3 cells, then the medium from the insert and the lower chamber was removed; the Transwell membrane was washed with PBS and 0.5 ml ethanol was added to solubilize the Cou-6 adsorbed on the membrane. The solution was collected and its fluorescence was read as reported above. The fluorescence was always less than 4% of the fluorescence measured in the lower chamber medium in all the experimental conditions, suggesting that such very low absorption of Cou-6 on the Transwell insert did not influence the results of the permeability assays.

The level of significance was determined by a Student's *t* test. Statistical significance was defined as $p < 0.001$.

2.10 In vitro cytotoxicity assay

For cytotoxicity studies, NO3 cells (both NS and AC) and CV17 NS were used at various passage numbers between 20 and 30, whereas 010627 cells (both NS and AC) were used at passage numbers between 160 and 180.

Free PTX (Sigma Aldrich Co., St. Louis, MO, USA) was dissolved in 100% DMSO for stock solutions and dilutions for cell treatments were made extemporaneously in culture medium, so that the final concentration of DMSO never exceeded 0.3% (v/v).

Cell lines were treated for 72 h with increasing doses (20, 100, 500, 1400 nM) of free PTX.

After exposure the cytotoxic effect of free Paclitaxel (PTX) and PTX-loaded SLN against tumor cells was evaluated assessing the number of viable cells by the Trypan blue dye exclusion test, using a TC20 automated cell counter (Bio-Rad, Berkeley, CA, USA). As for AC, results were confirmed by the 3-(4,5-dimethylthiazol-2-yl)-2,5-diphenyl-tetrazolium bromide (MTT) assay (Roche, Diagnostic Corporation Indianapolis, IN, USA) [43].

For Trypan blue assay, cells were plated at a density of 200×10^3 cells in 5 ml medium in a 25 cm^2 flask and treated with PTX (free in solution or encapsulated in SLN2, SLN9 or SLN15) at 37°C in 5% O_2/CO_2 for different times (24 and 72 h). Stock solutions were diluted extemporaneously in fresh medium at the desired concentration and administered to cells.

Cytotoxicity was expressed as number of surviving cells as percentage of control (untreated cells). For MTT assay, cells were seeded in 96-well plates (1×10^4 cells/well in 100 µl medium) and treated with the different concentrations and times above indicated of the drug (free or encapsulated) at 37 °C in 5% O_2/CO_2. The medium with the SLN was replaced with fresh medium and 10 µl of MTT solution (5mg/ml) were added to each well and incubated for 4 h at 37 °C. The extent of cell viability is indicated by mithocondrial conversion of yellow MTT, a tetrazole, to purple formazan by the living cells. Formazan crystals were solubilized overnight in 10% sodium dodecyl sulfate (SDS), 0.01 M HCl and optical density was measured at 570 nm (test wavelength) and 660 nm (reference wavelength) using a microplate spectrophotometer (Synergy HT, BioTek Instruments Inc., Winooski, VT, USA). Cell viability was expressed as a percentage of the absorbance measured in the treated cells compared to the control (untreated cells). All experiments were performed in quadruplicate.

The concentration of free PTX which caused a 50% cell growth inhibition (IC_{50}) compared with untreated controls, was calculated by non-linear regression for each cell line.

To investigate the cytotoxic effect of PTX incorporated in SLN, a drug concentration of 100 nM was chosen for the following *in vitro* experiments.

Cell viability was also measured after treatment with unloaded SLN (SLN2, SLN9 and SLN15) at the highest SLN concentration used for the study, *i.e.* 0.1% w/v.

The level of significance was determined by a two-tailed Student's *t* test. Statistical significance was defined as $p < 0.05$ or $p < 0.01$.

2.11 DNA damage/repair study by Immunofluorescence (IF)

The occurrence of a DNA damage after SLN treatment was investigated through the analysis by IF of γ-H2AX histone, that localizes at sites of DNA fragmentation as subnuclear foci.

The cell response to DNA insults was studied monitoring the activation of p-ATM, p-Chk2 and p-53BP1. HR or NHEJ repair system activities were analyzed through RAD51 or Ku70/Ku80 and DNA-PKcs proteins respectively. After 72 h treatment with unloaded SLN (SLN9) or with 100 nM PTX-loaded SLN9, cells were fixed for 20 minutes with 4% paraformaldehyde at room temperature, rinsed three times with PBS, blocked/permeabilized with PBS containing 2% of the appropriate serum and 0.1% Triton X-100 for 30 minutes and stained with the following primary antibodies: mouse anti-γ-H2AX (Ser139), mouse anti-p-ATM (Ser1981) (both from Millipore), rabbit anti-p-Chk2 (Thr68) (Cell Signaling Technology), rabbit anti-p-53BP1 (Ser25) (Bethyl Laboratories), mouse anti-RAD51, mouse anti-DNA-PKcs and mouse anti-Ku70/Ku80 (all from NeoMarkers). Negative controls were obtained by omitting the primary antibody. Alexa Fluor® 488-AffiniPure goat anti-rabbit IgG and Alexa Fuor® 594-AffiniPure rabbit anti-mouse IgG (Jackson ImmunoResearch Laboratories, Inc., West Grove, PA, USA) were used as secondary antibodies. Cell nuclei were counterstained with 4',6-diamidino-2-phenylindole (DAPI) and observations were made under a Zeiss Axioskop fluorescence microscope (Karl Zeiss, Oberkochen, Germany) equipped with an AxioCam5MR5c and coupled to an Imaging system (AxioVision Release 4.5; Karl Zeiss).

2.12 Specimen preparation for transmission electron microscopy (TEM)

Analysis by TEM was employed in order to get information on the possible ultrastructural modifications of cells treated with empty and PTX-loaded SLN. NO3 NS and AC lines were used for the investigation.

For transmission electron microscopy, untreated cells, cells treated with unloaded SLN15 and cells treated with 100 nM PTX-loaded SLN15 for 24 h were collected, pelleted by centrifugation and then fixed with 2.5% glutaraldehyde prepared in 0.1 M phosphate buffer at 4 °C. Samples were post-fixed with 1% osmium tetroxide for 2 h, dehydrated in a graded acetone series and embedded in the Epon 812 epoxy resin. Ultrathin sections were prepared using an ultracut microtome (Reichert-Jung, Germany), collected on copper grids, stained with both lead citrate and uranyl acetate, and then observed with a Philips CM-12 transmission electron microscope.

2.13 Glioblastoma cell cytotoxicity in co-culture models

In co-culture experiments, 500,000 glioblastoma cells (i.e. the U87-MG cell line and the primary human glioblastoma cells CV17 and 01010627) were added in the lower chamber of Transwells 4 days after seeding hCMEC/D3 cells in the upper chamber of Transwells. After 3 days of co-culture the medium of the upper chamber was replaced with fresh medium, with or without free PTX or PTX-loaded SLN (SLN 2) at different concentration (20, 50, 100, 200, 500 nM) for 24 h, as detailed under results.

To measure the viability of glioblastoma cells co-cultured with hCMEC/D3 cells, extracellular medium of glioblastoma cells was collected and centrifuged at 12,000 *g* for 15 min to pellet cellular debris, whereas cells were washed with fresh medium, detached with trypsin/EDTA (0.05/0.02% v/v), re-suspended in 0.2 ml of 82.3 mmol/l triethanolamine phosphate-HCl (pH 7.6) and sonicated on ice with two 10 s bursts (Labsonic sonicator, 100 W). LDH activity was measured in the extracellular medium and in the cell lysate: 50 µl of supernatant from extracellular medium or 5 µl of cell lysate were incubated at 37 °C with 5 mmol/l NADH. The reaction was started by adding 20 mmol/l pyruvic acid and was followed for 6 min, measuring absorbance at 340 nm with Packard

EL340 microplate reader (Bio-Tek Instruments, Winooski, VT). The reaction kinetics was linear throughout the time of measurement. Both intracellular and extracellular enzyme activity was expressed in μmol NADH oxidized/min/dish, then extracellular LDH activity was calculated as percentage of the total LDH activity in the dish.

The level of significance was determined by a Student's *t* test. Statistical significance was defined as $p < 0.05$, $p < 0.02$, $p < 0.01$, $p < 0.005$ or $p < 0.001$.

3. Results and discussion

As described in the introduction chapter, BBB is a physical barrier characterized by tight intracellular junctions and by the absence of fenestrations that limit permeability for therapeutic molecules with no exception for molecules in the glioblastoma treatment. The use of drug-loaded nanoparticles could be a winning strategy if an active targeting and a suitable drug concentration to the brain could be obtained, provided small-sized hydrophilic vehicles are achieved to prevent rapid degradation by reticuloendothelial system and carriers with proper superficial characteristics are coupled.

Moving from this background, SLN were prepared using the coacervation method which uses hydrophilic polymeric as stabilizers able to confer hydrophilic surface to SLN. Further to a cytotoxicity study against hCMEC/D3 cells relating to different fatty acids [40], BA was chosen as lipid matrix. In order to take advantages of possible interaction between BBB negative charges and surface positive-charged SLN, two positive charged molecules currently used in literature were introduced in the SLN preparation: ST [44] and GCS [36]. As antineoplastic model drug PTX was chosen, a lipophilic molecule suitable to be entrapped in SLN matrix.

Preliminary formulation studies (data not reported) demonstrated the need to modify the preparation procedure to obtain higher drug EE% by introducing PTX after SLN melting instead of adding it to the micellar solution; probably the high PTX lipophilicity does not allow its distribution within micelles, while promoting its solubilization in the molten lipid.

3.1 SLN characterization

In Table 1 compositions of PTX-loaded SLN are reported. SLN composition was the result of a preliminary screening carried out in a previous work [45].

In Table 1 ST-SLN and GCS-SLN compositions are also reported. Different formulations were obtained varying the amount of PVA 9000, ST, GCS or PTX in order to obtain the most suitable PTX vehicle as concerns Zeta potential, mean sizes, EE%, over time stability. In order to improve

460 SLN stability, CHOL was also added. As reported in literature [46] high CHOL/lipid ratio matrix
461 reduced mean diameters of SLN prepared from emulsion. This led to a rigid surfactant layer with
462 decrement in van der Waals attraction and promotion of net repulsion forces between oil droplets;
463 therefore, agglomeration and coalescence of small oil droplets were reduced. In addition, the
464 interaction between CHOL and surface active agent might increase the surface curvature of oil
465 droplets consequently leading to small size of SLN after cooling down. A similar behavior can be
466 hypothesized also in SLN obtained by coacervation. In the present experimental conditions, CHOL
467 probably might interact with Na-BA at the interface of micelles.
468 In Table 1 SLN, ST-SLN and GCS-SLN mean diameter and Zeta potential are reported. Most SLN
469 tested had sizes below 600 nm. In the neutral SLN series (SLN 0-3), increasing the amount of PTX
470 no changes in particles dimension were noted; different behavior was noted in the case of charged
471 SLN. In the ST-SLN series (SLN 4-10) an increase in diameter sizes can be noted when ST or PTX
472 amounts were increased or when CHOL was introduced in the formulation. Nevertheless the
473 presence of CHOL was essential to SLN stability: in the absence of CHOL, ST-SLN and GCS-SLN
474 showed a sudden increase in mean size immediately after preparation. Instead, in the GCS-SLN
475 (SLN 11-17) series a slightly decrease in SLN size was obtained increasing the GCS amount and a
476 more marked increase was noted when a great amount of stabilizer (PVA) was used. Also in this
477 case the presence of CHOL was necessary to formulations stability; the addition of this component
478 led to a decrease in mean diameter and the smallest SLN were obtained using 50 mg (1% w/w)
479 PVA (SLN 17).
480 The dissimilar influence of ST and GCS on ST-SLN and GCS-SLN sizes might be due to different
481 positioning of both charged molecules: probably, lipophilic ST chain was incorporated in the lipid
482 matrix while GCS was mainly adsorbed to the external surface of nanoparticles.
483 Size measurements were employed also diluting the samples with growth medium used in the in
484 vitro experiments in order to verify SLN sizes when they are tested in vitro. The growth medium
485 does not seem to influence SLN dimensions: all SLN have maintained their size (data not reported).

In Figures 1a and 1b TEM PTX-SLN2 images at different magnifications were reported. The SLN have spherical shape and sizes between 300 and 500 nm. The drug introduction does not seem to affect shape and size (data not reported). Similar characteristics were obtained also with SLN9 and SLN15.

The observation of Cou-6-SLN nanosuspensions under optical microscope confirmed both the spherical shape and the dimensional range of the particles. The use of fluorescent light allowed to locate Cou-6 in SLN nanosuspensions: homogeneous dispersions of fluorescent nanoparticles were observed with all formulations (data not shown).

In Table 1 also Zeta potential values are reported. All GC or ST-containing formulations showed positive charge with values in the 7.6 - 23.8 mV range. ST-SLN presented Zeta potential ranging from 7 to 15 mV (depending on ST amount used); these values are smaller than those of GCS-SLN and those of SLN containing the same ST percentages but prepared with methods other than coacervation [41]; probably PVA 9000 used as stabilizer locates itself externally thus partially screening the ST positive charge.

In GCS-SLN series, Zeta potential values confirmed the external positioning of the polymer: probably positively-charged GCS interacted with carboxylate groups on SLN surface, conferring them a positive charge. The values were influenced by GCS amount: by increasing the polymer an increase of Zeta potential from 16.9 mV to 23.8 mV was noted; the presence of CHOL and the PTX amount variation did not seem to influence this parameter.

In Table 2 the amount of PTX in SLN is expressed as EE% and as loading (mg PTX/mg BA). Almost all tested SLN showed a good PTX loading capacity; in particular, in neutral SLN series (SLN 0-3) PTX EE% did not significantly vary increasing the drug amount, while drug loading was increased over twice folds. In the ST-SLN series (SLN 4-10), PTX EE% was significantly influenced by several factors. Increasing ST amounts determined a reduction of PTX EE% (SLN 5) which was partially counteracted by the presence of CHOL (SLN 6) probably as a consequence of a

hardened structure of SLN surface. Also PVA amount seemed to be relevant in influencing PTX EE%, as higher PVA concentrations determined a reduction in PTX EE%.

In GCS-SLN series (SLN 11-17), EE% and PTX loading ranged from 24% to 83% and from 1.4 to 5.0 mg/mg BA respectively. Also in this series PTX EE% was strongly influenced by PVA 9000 amount: when the highest stabilizer amount was used (SLN 14), a dramatic decrease in drug EE% up to 24% can be noted; probably PVA 9000 formed micelles in aqueous phase able to solubilize PTX. CHOL introduction enhanced PTX EE% from 52% to 75% particularly in SLN prepared with 50 mg PVA 9000. On the contrary, GCS amount variations did not seem to affect drug EE%.

To mime SLN behavior after administration when they are diluted in physiological fluids, drug EE% was determined also after 1:100 dilutions. When water was used as dilution medium, EE% remained almost unvaried in all ST-SLN (±1%), except in SLN 15 in which a 10% decrease was registered. Probably, in GCS-SLN, PTX is partially trapped in GCS chains located on SLN surface and therefore it might be released upon high dilutions. To evaluate the influence of different dilution media, SLN 9, which were chosen as those having the best properties for our experimental purposes, were diluted also by pH 7.4 PBS and pH 5.5 citric buffer. No significant variation was noted upon dilution by pH 7.4 PBS (±1%), while a certain PTX amount was released when 0.1 citric pH 5.5 buffer was used, that mimed the lysosomial environment: the EE% decreased from 92% to 77% and this could be due to a PTX slow release.

3.2 SLN and PTX stability

The studies were carried out only on SLN giving the best results concerning sizes and EE%. The chosen formulations were analyzed to verify their stability overtime. The results are reported in Table 3. SLN 9 showed a great increase in mean diameter (up to 1500 nm) after 30 days, while only a slight decrease occurred in EE%. The poor dimensional stability of SLN 9 could be due to their low Zeta potential (about 9 mV) which is probably not sufficient to prevent SLN aggregation. On the other hand, GCS-SLN (SLN 15, 16, 17) showed a higher dimensional stability although a

gradual increase in mean diameter and a gradual decrease in Zeta potential were registered due probably to a slow solubilization of the external GCS coating in the aqueous phase.

To overcome the poor stability of SLN suspension and to find an optimal storage method, they were submitted to freeze drying. In Table 4 SLN sizes after freeze-drying were reported. The freeze-drying process was carried out without adding any cryoprotectant; in fact in a previous work [45] PVA 9000 was found to be able to protect SLN during freeze-drying as well as 2% threalose.

The characterization of resulting SLN suspensions showed a mean diameter increase of all SLN analyzed probably due to a partial SLN aggregation. This increase was about 300 nm in SLN with ST while only a slight variation was registered in SLN with GCS; probably also GCS, positioning externally, could behave as cryoprotectant preventing nanoparticles aggregation. The smallest increase (about 40 nm) was noted when higher amounts of stabilizer were used. EE% was kept constant in almost all preparations; an increase in EE% (from 75% up to 89%) was registered in SLN 17 that presented a higher amount of free PTX: probably during freeze-drying a part of free PTX was internalized or absorbed onto nanoparticles.

3.3 Determination of PTX release

In Figure 2 PTX release plots from SLN using the dialysis method were reported. In this experiment drug diffusion through the dialysis membrane was influenced by drug release rate from SLN. As it can be seen, PTX was released very slowly from SLN: less than 1% PTX was released from SLN formulations in 12 hours while, at the same time, about 40% PTX diffused from PTX solution. This slow release could confirm PTX incorporation into SLN. From the $K_{d\ app}$ data it could be seen as PTX release from GCS-SLN was still slower than from ST-GCS; these results could be the confirmation that GCS formed an external coating that further limited drug release.

3.4 Permeability of SLN across BBB

As shown in Figure 3, the permeability of free Cou-6 across the hCMEC/D3 monolayer remained very low at all the time points considered; the permeability of Cou-6-loaded SLN was similar to that of free Cou-6 after 0,5 h, but became significantly higher after 3 h and 24 h. Apparently there were no differences in the permeability of uncharged SLN (SLN 2) versus positively charged SLN (SLN 9 and SLN 15), although SLN 9 resulted the best permeable formulation after 24 h.

3.5 In vitro cytotoxicity studies

To assess the sensitivity of the five malignant glioma cell lines to PTX, we treated previously the cells with Cremophor® EL:ethanol 50:50 drug solution (free PTX) at concentrations ranging from 20 nM to 1.4 μM for 72 h.

After different exposure times both MTT and trypan blue assays were performed. PTX was able to block *in vitro* cellular proliferation in a dose-dependent manner; it inhibited clonogenic growth of NS (Figure 4a–4d) and hindered adhesion process in AC (Figure 4e–4i).

The growth inhibitory effect was more evident on AC than on NS.

The IC_{50} values of free PTX at 72 h for the three NS cell lines studied were < 20 nM; for the two AC lines were < 15 nM (Figure 5). Consequently, drug concentration of 100 nM was employed for the following experiments with PTX incorporated in SLN. At this dosage, a statistically significant decrease of cell viability was caused by PTX compared with untreated cells, both as free drug and as SLN-carried, and this effect increased prolonging drug exposure time from 24 to 72 h. It was observed that also PTX encapsulated in SLN caused inhibition of sphere formation in the NS cultures (Figure 4e) and interfered with cell adhesion in AC cultures (Figure 4l).

Graphs in Figure 7 show cell viability of NO3 line after the treatments: as regards NS, the viable cell number decreased to 60-70% after 24 h treatment with the different PTX-SLN (Figure 6a) and to 30-40% after 72 h treatment (Figure 6b). At 24 h free PTX and all PTX-SLN gave a cytotoxicity statistically different from control, while only SLN 2 produced an increase in cytotoxicity

588 significantly different from that of empty SLN 2. Prolonging the incubation time, also SLN 9 were
589 significantly different from the corresponding empty SLN.
590 The reduction of viability of AC was about 10-15% higher than the one of NS (Figure 7). An
591 analogous behavior of PTX-SLN 2 and PTX-SLN 9 was noted already after 24 h incubation, while
592 after 72 h all SLN under study produced a cytotoxicities significantly different from those produced
593 by the corresponding empty SLN. The cytotoxicity of PTX incorporated in SLN appeared similar
594 or even slightly higher in comparison with the one of free drug solution. In particular, SLN2 seemed
595 to enhance growth inhibitory activity of PTX on NS lines, while SLN 9 did it on AC lines.
596 The results slightly varied in the other cell lines (data not shown), but the cytotoxic activity of PTX-
597 loaded SLN remained always equal or greater compared with free drug. SLN 2 and SLN 9 appeared
598 as the most effective carrier formulations.
599 Control experiments demonstrated that the exposure of the cells with the unloaded SLN at the
600 highest SLN concentration used for the study determined a mild reduction of cell viability too,
601 mostly on AC. Unloaded SLN 2 formulation displayed the smallest cytotoxic effect, while unloaded
602 SLN15 had a more accentuated action on cell proliferation.
603 Treatment with PTX vehicle (50:50 v/v mixture of Cremophor® EL and ethanol) at the same
604 concentrations used for drug solutions showed a slight cytotoxicity too (data not reported).
605 Our results suggest that, first of all, incorporation of PTX in SLN did not alter its cytotoxic
606 capability and that these carriers, thanks to a good cell membrane permeation, are able to efficiently
607 transport the drug inside the cells. Encapsulation into SLN appeared even to enhance the growth
608 inhibitory effect of PTX on GBM cell lines.
609 In conclusion, loading of PTX in SLN seems to sensitize cells and to decrease their resistance to the
610 drug.
611
612 *3.6 Study of PTX-SLN cytotoxic effect by TEM*

The observation by TEM enabled to evaluate the ultrastructural alterations of cells after exposure to SLN. The analysis revealed that the administration of unloaded SLN 15 didn't cause modifications to the cell morphology both in NS and in AC. Cells treated with empty SLN maintained unchanged nucleus, ergastoplasma, Golgi apparatus and mithocondria (Figure 8a).

On the contrary, 24 h exposure to SLN loaded with 100 nM PTX induced severe alterations of the cellular morphology that included cytoplasmic accumulation of vacuoles, loss of mitochondrial ridges and finally mithocondrial lysis (Figure 8b-8f). The vacuoles became gradually larger and confluent and in some cases they blended and formed autophagolysosomes surrounded by a membrane. Cytoplasmic rarefaction, glycogen accumulation and destruction of all organelles suggested a typical regressive apoptotic pattern. Only in some areas there was evidence of SLN residues. These results indicate an evident cell damage caused by the PTX vehicled in the SLN.

3.7 DNA damage and repair response induced by PTX-SLN treatment

In response to DNA damage caused by genotoxic agents, the eukaryotic cell activates a complex checkpoint/repair pathway in order to repair the lesion before replication. The signalling involves the recruitment of the sensor protein kinase ataxia telangiectasia mutated (ATM), that initiates a transduction cascade phosphorylating downstream effectors, including H2AX histone, 53 binding protein 1 (53BP1) and the checkpoint kinases 1 and 2 (Chk1 and Chk2). When checkpoints are activated, the cell cycle is halted to allow DNA repair. If the damage is too severe, repair fails and the cell enters into apoptosis [47]. Two are the major pathways used by mammalian cells to repair double strand break damage: the homologous recombination (HR), which takes place during the S and G2 phases and is driven mainly by RAD51 protein, and the non-homologous end joining (NHEJ), which occurs during G0 and G1 phases. The key NHEJ effector is DNA-dependent protein kinase (DNA-PK), which consists of a regulatory subunit (Ku70/Ku80 heterodimer) and a catalytic subunit (DNA-PKcs) [48]. In glioma cells, increased DNA damage response and repair ability contribute to determine the radio- and chemoresistant phenotype of these cells [49].

After glioma cell treatment for 72 h with relatively high concentration (100 nM) of free PTX we observed a moderate activation of checkpoint and repair proteins. A mild expression of all markers, was found both in NS and in AC (data not shown), indicating that this drug is able to induce genotoxic lesions.

Even after NO3 cell line treatment with PTX carried by SLN, we found the presence of γ-H2AX positive-nuclei and a moderate expression of all sensors and effectors of checkpoint/repair pathway, both in NS (Figure 9a-9g) and in AC (Figure 9l-9q), demonstrating that the encapsulated drug maintains the ability to induce a DNA strand break damage in the glioma cell lines. As already observed for the free drug, mostly on AC lines, several cells treated with PTX-SLN appeared blocked in metaphasis (Figure 9i) and presenting a strong expression of the checkpoint/repair proteins (p-ATM, p-Chk2, p-53BP1, γ-H2AX, DNA-PKcs). It seemed from these findings that cells try to repair the genotoxic lesions mainly through the NHEJ system. Untreated cells were negative for all markers (inserts in Figure 9a and 9i are examples for p-ATM expression).

After exposure of cells to unloaded SLN for 72 h we did not observe positivity of any checkpoint/repair protein (panels h and r of Figure 9 are examples for p-ATM expression).

3.8 Effective cytotoxicity of paclitaxel-loaded SLN against glioblastoma cells in co-culture models.

The cytotoxicity of PTX-loaded SLN on glioblastoma cells was finally compared with that of free PTX in co-culture models of hCMEC/D3 cells and glioblastoma cells. As shown in Figures 10, 11 and 12, free PTX induced a dose-dependent increase of cytotoxicity in all the glioblastoma cell lines; PTX-loaded SLN followed a similar trend and showed – at the same concentration – higher efficacy than the free drug. Also the toxicity on hCMEC/D3 cells increased dose-dependently, without significant differences between free PTX and PTX-loaded SLN (Figure 13).

By comparing the cytotoxicity profile on glioblastoma cells and hCMEC/D3 cells, we can state that PTX-loaded SLN achieves significant toxicity against tumor cells at concentrations that are not toxic for BBB cells. To obtain the same degree of cytotoxicity on glioblastoma cells, free PTX

665 should be used at concentration that are unacceptably toxic for brain microvascular endothelial
666 cells. The different efficacy of free versus SLN-loaded PTX can be explained by the increased
667 permeability of the latter through the BBB monolayer. PTX is a known substrate of P-glycoprotein
668 (Pgp) [50], which is abundant on the luminal side of BBB cells [51]; therefore, it is a poorly
669 delivered drug into the brain parenchima. Its loading within SLN may represent a valid strategy to
670 overcome the efflux by Pgp at BBB levels.
671 In addition, also glioblastoma has been reported to be rich of Pgp [52] and multidrug resistance
672 related protein 1 (MRP1) [53], a second protein that actively effluxes PTX [50], limiting its
673 intracellular accumulation and toxicity. Therefore, a lower accumulation and toxicity of paclitaxel is
674 expected within glioblastoma cells. The loading within SLN may promote a faster uptake and/or a
675 lower efflux by Pgp and MRP1 from glioblastoma cells as well. Therefore, the loading in SLN may
676 represent a valid strategy to simultaneously bypass the drug efflux at BBB and glioblastoma levels.

4. Conclusion

The fatty acid coacervation technique, a solvent free method, was used to prepare PTX-loaded SLN. The use of positive-charged molecules, such as ST and GCS, allowed to obtain positive SLN with sizes in the 300-600 nm range and PTX EE% in the 25-90% range.

Permeability studies through hCMEC/D3 cells monolayer, assumed as *in vitro* model of the BBB, showed a significantly increase in the permeation of Cou-6, used as model drug, when vehicled in SLN; no significantly differences in the permeability of uncharged SLN versus positively charged SLN were noted after 24 h.

Cytotoxicity studies on NO3 glioblastoma cell line demonstrated the absence of toxicity of unloaded SLN 2 and 9 and the preservation of cytotoxic activity of PTX-loaded SLN that remained always equal or greater compared with free drug.

In co-culture experiments with hCMEC/D3 and different glioblastoma cells, it was demonstrated that, when delivered in SLN, PTX increased its cytotoxicity towards glioblastoma cells, because of its increased permeation through the endothelial cell monolayer.

According to these *in vitro* results, the positive charge did not seem essential to enhance PTX brain uptake but fundamental seem to be the PTX encapsulation into SLN.

Further i.v. administration of PTX-loaded SLN in rats are in progress to confirm the suitability of SLN in enhancing PTX overcoming of the BBB.

Acknowledgements

The authors wish to acknowledge Compagnia di San Paolo, under the research project "Development of solid lipid nanoparticles (SLN) as vehicles of antineoplastic drugs to improve the pharmacological glioblastoma therapy" (ORTO11WINST).

References

[1] M.K. Nicholas, R.V. Lukas, S. Chmura, B. Yamini, M. Lesniak, P. Pytel, Molecular heterogeneity in glioblastoma: therapeutic opportunities and challenges, Semin. Oncol. 38 (2011) 243–253.

[2] M. Weller, Novel diagnostic and therapeutic approaches to malignant glioma, Swiss Med. Wkly. 141 (2011) doi:10.4414/smw.2011.13210

[3] W. Loscher, H. Potschka, Drug resistance in brain diseases and the role of drug efflux transporters, Nat. Rev. Neurosci., 6 (2005), 591-602.

[4] B.T. Hawkins, T.P. Davis, The blood-brain barrier/neurovascular unit in health and disease, Pharmacol. Rev. 57 (2005), 173-185.

[5] N.R. Saunders, C.J. Ek, M.D. Habgood, K.M. Dziegielewska, Barriers in the brain: a renaissance?, Trends Neurosci. 31 (2008), 279-286.

[6] M.L. Pinzón-Daza, I. Campia, J. Kopecka, R. Garzón, D. Ghigo, C. Riganti. Nanoparticle- and liposome-carried drugs: new strategies for active targeting and drug delivery across blood-brain barrier, Curr. Drug Metab. 14 (2013), 625-640.

[7] M.W. Brightman, T.S. Reese, Junctions between intimately apposed cell membranes in the vertebrate brain, J. Cell. Biol. 40 (1969) 648–677.

[8] A. Béduneau, P. Saulnier, J. Benoit, Active targeting of brain tumors using nanocarriers, Biomaterials 28 (2007) 4947–4967.

[9] M.S. Lesniak, U. Upadhyay, R. Goodwin, B. Tyler, H. Brem, Local delivery of doxorubicin for the treatment of malignant brain tumors in rats, Anticancer Res. 25 (2005) 3825–3831.

[10] T.F. Cloughesy, K.L. Black, Pharmacological blood–brain barrier modification for selective drug delivery, J. Neuro-Oncol. 26 (1995) 125–132.

[11] A.A. Sinkula, S.H. Yalkowsky, Rationale for design of biologically reversible drug derivatives: prodrugs, J. Pharm. Sci. 64 (1975) 181–210.

725 [12] E. Garcia-Garcia, K. Andrieux, S. Gil, P. Couvreur, Colloidal carriers and blood–brain barrier
726 (BBB) translocation: A way to deliver drugs to the brain? Int. J. Pharm. 298 (2005) 274–292.
727 [13] M.I. Alam, S. Beg, A. Samad, S. Baboota, K. Kohli, J. Ali, A. Ahuja, M. Akbar, Strategy for
728 effective brain drug delivery, Eur. J. Pharm. Sci. 40 (2010) 385–403.
729 [14] J. Kreuter, Nanoparticulate systems for brain delivery of drugs, Adv Drug Deliver Rev 47,
730 (2001) 65-81.
731 [15] P.R. Lockman, J.M. Koziara, R.J. Mumper, D.D. Allen, Nanoparticle surface charges alter
732 blood–brain barrier integrity and permeability, J. Drug Target. 12 (2004) 635–641.
733 [16] K. Park, Transport across the blood–brain barrier using albumin nanoparticles, J. Control.
734 Release 137 (2009) 1.
735 [17] A. Mistrya, S. Stolnika, L. Illum, Nanoparticles for direct nose-to-brain delivery of drugs, Int.
736 J. Pharm. 379 (2009) 146–157.
737 [18] J. Kreuter, P. Ramge, V. Petrov, S. Hamm, S.E. Gelperina, B. Engelhardt, R. Alyautdin, H.
738 Von Briesen, D.J. Begley, Direct evidence that polysorbate-80-coated poly(butylcyanoacrylate)
739 nanoparticles deliver drugs to the CNS via specific mechanisms requiring prior binding of drug to
740 the nanoparticles, Pharm. Res. 20 (2003) 409–416.
741 [19] A.E. Gulyaev, S.E. Gelperina, I.N. Skidan, A.S. Antropov, G.Y. Kivman, J. Kreuter,
742 Significant transport of doxorubicin into the brain with polysorbate 80-coated nanoparticles, Pharm.
743 Res. 16 (1999) 1564–1569.
744 [20] J. Kreuter, R.N. Alyautdin, D.A. Kharkevich, A.A. Ivanov, Passage of peptides through the
745 blood–brain barrier with colloidal polymer particles (nanoparticles), Brain Res. 674 (1995) 171–
746 174.
747 [21] S.S. Feng, L. Mu, K.Y. Win, G. Huang, Nanoparticles of biodegradable polymers for clinical
748 administration of paclitaxel, Curr. Med. Chem. 11 (2004), 413–424.

749 [22] J.M. Koziara, P.R. Lockman, D.D. Allen, R.J. Mumper, Paclitaxel nanoparticles for the
750 potential treatment of brain tumors, J. Control. Release 99 (2004) 259–269.
751 [23] J.F. Poduslo, G.L. Curran, Polyamine modification increases the permeability of proteins at the
752 blood–nerve and blood–brain barriers, J. Neurochem. 66 (1996) 1599–1609.
753 [24] Z. Nagy, H. Peters, I. Huttner, Charge-related alterations of the cerebral endothelium, Lab.
754 Invest. 49 (1983) 662–671.
755 [25] J.E. Hardebo, J. Kahrstrom, Endothelial negative surface charge areas and blood–brain barrier
756 function, Acta Physiol. Scand. 125 (1985) 495–499.
757 [26] L. Fenart, A. Casanova, B. Dehouck, C. Duhem, S. Slupek, R. Cecchelli, D. Betbeder,
758 Evaluation of effect of charge and lipid coating on ability of 60-nm nanoparticles to cross an in
759 vitro model of the blood–brain barrier, J. Pharmacol. Exp. Ther. 291 (1999) 1017–1022.
760 [27] W. Lu, Y. Zhang, Y. Tan, K. Hu, X. Jiang, S. Fu, Cationic albumin-conjugated pegylated
761 nanoparticles as novel drug carrier for brain delivery, J. Control. Release 107 (2005) 428–448.
762 [28] P. Blasi, A. Schoubben, G. Traina, G. Manfroni, L. Barberini, P.F. Alberti, C. Cirotto, M.
763 Ricci, Lipid nanoparticles for brain targeting III. Long-term stability and in vivo toxicity, Int. J.
764 Pharm. 454 (2013) 316–323.
765 [29] M. Patel, E.B. Souto, K.K. Singh, Advances in brain drug targeting and delivery: limitations
766 and challenges of solid lipid nanoparticles, Expert Opin. Drug Deliv. 10 (2013) 889-905.
767 [30] M.J. Glantz, M.C. Chamberlain, S.M. Chang, M.D. Prados, B.F. Cole, The role of paclitaxel in
768 the treatment of primary and metastatic brain tumors, Semin. Radiat. Oncol. 9 (1999) 27–33.
769 [31] S.H. Tseng, M.S. Bobola, M.S. Berger, J.R. Silber, Characterization of paclitaxel (Taxol)
770 sensitivity in human glioma- and medulloblastoma-derived cell lines, Neuro-Oncology 1 (1999)
771 101–108.

772 [32] A. Desai, T. Vyas, M. Amiji, Cytotoxicity and apoptosis enhancement in brain tumor cells
773 upon coadministration of paclitaxel and ceramide in nanoemulsion formulations, J. Pharm. Sci. 97
774 (2008) 2745–2756.
775 [33] S. Fellner, B. Bauer, D.S. Miller, M. Schaffrik, M. Fankhaenel, T. Spruh, G. Bernhardt, C.
776 Graeff, L. Faerber, H. Gschaidmeier, A. Buschsuer, G. Fricker, Transport of Paclitaxel (Taxol)
777 across the blood–brain barrier in vitro and in vivo, J. Clin. Invest. 10 (2002) 1309–1317.
778 [34] P. Ma, R.J. Mumper**,** Paclitaxel Nano-Delivery Systems: A Comprehensive Review, J
779 Nanomed Nanotechol 4 (2013) doi:10.4172/2157-7439.1000164
780 [35] L. Battaglia, M. Gallarate, R. Cavalli, M. Trotta, Solid lipid nanoparticles produced through a
781 coacervation method, J. Microencapsul. 27 (2010) 78–85.
782 [36] A. Trapani, J. Sitterberg, U. Bakowsky, T. Kissel, The potential of glycol chitosan
783 nanoparticles as carrier for low water soluble drugs, Int. J. Pharm. 375 (2009) 97–106.
784 [37] S. Mao, W. Sun, T. Kissel, Chitosan-based formulations for delivery of si-RNA and DNA
785 systems for protein therapeutics and antigens, Adv. Drug Del. Rev. 62 (2010) 12–27.
786 [38] B.B. Weksler, E.A. Subileau, N. Perrière, P. Charneau, K. Holloway, M. Leveque, H. Tricoire-
787 Leignel, A. Nicotra, S. Bourdoulous, P. Turowski, D.K. Male, F. Roux, J. Greenwood, I.A.
788 Romero, P.O. Couraud, Blood-brain barrier-specific properties of a human adult brain endothelial
789 cell line, Faseb. J. 19 (2005) 1872-1874.
790 [39] C. Riganti, I.C. Salaroglio, M.L. Pinzòn-Daza, V. Caldera, I. Campia, J. Kopecka, M. Mellai,
791 L. Annovazzi, P.O. Couraud, A. Bosia, D. Ghigo, D. Schiffer, Temozolomide down-regulates P-
792 glycoprotein in human blood-brain barrier cells by disrupting Wnt3-signalling, Cell Mol Life Sci
793 71 (2014) 499-516.
794 [40] V. Caldera, M. Mellai, L. Annovazzi, A. Piazzi, M. Lanotte, P. Cassoni, D. Schiffer, Antigenic
795 and Genotypic Similarity between Primary Glioblastomas and Their Derived Neurospheres, J.
796 Oncol. ID 314962 (2011) doi:10.1155/2011/314962.

797 [41] M. Trotta', E. Peira, M.E. Carlotti, M. Gallarate, Deformable liposomes for dermal
798 administration of methotrexate, Int. J. Pharm. 270, (2004) 119-125.
799 [42] L. Battaglia, M. Gallarate, E. Peira, D. Chirio, E. Muntoni, E. Biasibetti, M.T. Capucchio, A.
800 Valazza, P.P. Panciani, M. Lanotte, D. Schiffer, L. Annovazzi, V. Caldera, M. Mellai, C. Riganti,
801 Solid lipid nanoparticles for potential doxorubicin delivery in glioblastoma treatment: preliminary
802 i*n vitro* studies, J. Pharm. Sci. (2014) doi:10.1002/jps.24002.
803 [43] T.R. Mosmann, Rapid colorimetric assay for cellular growth and survival: application to
804 proliferation and cytotoxicity assay, J. Immunol. Methods 65 (1983) 55–63.
805 [44] D. Pandita, A. Ahuja, V. Lather, T. Dutta, T. Velpandian, R.K. Khar, Development,
806 characterization and *in vitro* assessement of strearylamine-based lipid nanoparticles of paclitaxel.
807 *Pharmazie* 66 (2010) 171-177.
808 [45] D. Chirio, M. Gallarate, E. Peira, L. Battaglia, L. Serpe, M. Trotta, Formulation of curcumin-
809 loaded solid lipid nanoparticles produced by fatty acids coacervation technique, J. Microencapsul.
810 28 (2011) 537-548.
811 [46] R. Asasutjarit, S. Lorenzen, S. Sirivichayakul, K. Ruxrungtham, U. Ruktanonchai, G.C.
812 Ritthidej, Effect of solid lipid nanoparticles formulation compositions on their size, zeta potential
813 and potential for in vitro pHIS-HIV-hugag, Transfection. Pharm. Res. 24 (2007) 1098-1107.
814 [47] E. Bolderson, D.J. Richard, B.B. Zhou, K.K. Khanna, Recent advances in cancer therapy
815 targeting proteins involved in DNA double-strand break repair, Clin. Cancer Res. 15 (2009) 6314–
816 6320.
817 [48] B. Pardo, B. Gómez-González, A. Aguilera, DNA repair in mammalian cells: DNA double-
818 strand break repair: how to fix a broken relationship, Cell. Mol. Life Sci. 66 (2009) 1039–1056.
819 [49] T.C. Johannessen, R. Bjerkvig, B.B. Tysnes, DNA repair and cancer stem-like cells--potential
820 partners in glioma drugresistance?, Cancer Treat. Rev. 34 (2008) 558–567.

[50] S. Agarwal, R. Sane, R. Oberoi, J.R. Ohlfest, W.F. Elmquist, Delivery of molecularly targeted therapy to malignant glioma, a disease of the whole brain, Expert Rev. Mol. Med. 13:e17 (2011) doi: 10.1017/S1462399411001888.

[51] L.M. Tai, A.J. Loughlin, D.K. Male, I.A. Romero, P-glycoprotein and breast cancer resistance protein restrict apical-to-basolateral permeability of human brain endothelium to amyloid-β, J. Cereb. Blood F. Met. 29 (2009) 1079-1083.

[52] A. Salmaggi, A. Boiardi, M. Gelati, A. Russo, C. Calatozzolo, E. Ciusani, F.L. Sciacca, A. Ottolina, E.A. Parati, C. La Porta, G. Alessandri, C. Marras, D. Croci, M. De Rossi, GBM-derived tumorospheres identify a population of tumor stem-like cells with angiogenic potential and enhanced multidrug resistance phenotype, Glia 54 (2006) 850–860.

[53] E. Nakai, K. Park, T. Yawata, T. Chihara, A. Kumazawa, H. Nakabayashi, K. Shimizu, Enhanced MDR1 expression and chemoresistance of cancer stem cells derived from GBM. Cancer Invest. 27 (2009) 901–908.

FIGURE CAPTIONS

Figure A.1: Anatomical structures composing the BBB. AJs: adherent junctions. TJs: tight junctions. ABC: ATP binding cassette transporters.

Figure 1: TEM images. a) 2200X magnification; b) 8900X magnification.

Figure 2: PTX release plots from nanoparticles using the dialysis method

Figure 3: Cou-6 permeability 0.1% dilution. * $p < 0.001$

Figure 4: Effect of 72 h treatment with increasing doses (100, 500, 1400 nM) of free and 100 nM SLN10-encapsulated PTX on NO3 NS (b–e) and NO3 AC (g–k) growth. Control cells (a, f) did not receive any treatment. All 200x magnification.

Figure 5: Cytotoxicity of free PTX on NS (A) and AC (B) of NO3 glioma cell line at various dosages of drug (20, 100, 500, 1400 nM) after 72 h treatment.

Figure 6: a) cell viability of NO3 NS after 24 h treatment; b) cell viability of NO3 NS after 72 h treatment + $p < 0.05$ vs CTRL; * $p < 0.05$ PTX-SLN vs SLN; ++ $p < 0.01$ vs CTRL; ** $p < 0.01$ PTX-SLN vs SLN

Figure 7: a) cell viability of NO3 AC after 24 h treatment; b) cell viability of NO3 AC after 72 h treatment ++ $p < 0.01$ vs CTRL; * $p < 0.05$ PTX-SLN vs SLN;

Figure 8: TEM of NS after treatment with SLN15 at 15000 x. (a) After 24 h treatment with unloaded SLN15. (b) After 6 h treatment with 100 nM PTX-loaded SLN15 (c) After 24 h treatment with 100 nM PTX-loaded SLN15 (d) Id, large vacuoles surrounded by a membrane, (e) Id, autophagolysosomes, 15000 x. (f) Possible remnants of SLN (20000 x).

Figure 9: Expression by IF of checkpoint/repair proteins in NO3 glioma cells after 72 h treatment with 100 nM PTX-loaded SLN10: p-ATM, 200x (a), γ-H2AX, 200x (b), p-Chk2, 200x (c), p-53BP1, 200x (d), DNA-PKcs, 200x (e), Ku70/80, 200x (f), RAD51, 200x (g) in NS; AC arrested in metaphases, DAPI, 200x (j); p-ATM, 200x (k), γ-H2AX foci, 400x (i), p-Chk2, 200x (l), p-53BP1, 200x (m), DNA-PKcs, 200x (n), RAD51, 200x (o) in AC; nuclei counterstained with DAPI. Negative reaction for p-ATM in untreated NS and AC, respectively (upper and lower left inserts of panels a and i) and in NS and AC treated with unloaded SLN for 72 h (h and p); nuclei counterstained DAPI, 200x.

Figure 10: cytotoxicity against CV17 cells. + $p < 0.05$ vs CTRL; ++ $p < 0.02$ vs CTRL; +++ $p < 0.01$ vs CTRL; ++++ $p < 0.005$ vs CTRL; +++++ $p < 0.001$ vs CTRL; * $p < 0.05$ SLN vs PTX; ** $p < 0.02$ SLN vs PTX; *** $p < 0.001$ SLN vs PTX.

Figure 11: cytotoxicity against O625 cells. + $p < 0.05$ vs CTRL; ++ $p < 0.02$ vs CTRL; +++ $p < 0.01$ vs CTRL; ++++ $p < 0.005$ vs CTRL; +++++ $p < 0.001$ vs CTRL; * $p < 0.05$ SLN vs PTX.

Figure 12: cytotoxicity against U87 cells. + $p < 0.01$ vs CTRL; ++ $p < 0.002$ vs CTRL; +++ $p < 0.005$ vs CTRL; * $p < 0.05$ SLN vs PTX; ** $p < 0.02$ SLN vs PTX; *** $p < 0.001$ SLN vs PTX.

Figure 13: cytotoxicity against hCMEC/D3 cells. + $p < 0.01$ vs CTRL; ++ $p < 0.005$ vs CTRL * $p < 0.05$ SLN vs PTX; ** $p < 0.002$ SLN vs PTX.

885

SLN	Na-BA* (mg)	PVA 9000 (mg)	PTX (mg)	CHOL (mg)	ST (mg)	GCS (mg)	Mean diameter (nm) (PDI)	Zeta Potential (mV)
0	53	37.5	3	-	-	-	299.2 ± 0.3 (0.053)	- 3.04 ± 0.56
1	53	37.5	3	0.5	-	-	381.3 ± 20.4 (0.152)	- 3.30 ± 0.47
2	53	37.5	4.5	0.5	-	-	386.4 ± 12.3 (0.167)	- 3.34 ± 0.79
3	53	37.5	6	0.5	-	-	383.8 ± 23.2 (0.085)	- 3.41 ± 0.60
4	53	37.5	3	-	3	-	345.6 ± 9.7 (0.089)	7.85 ± 0.91
5	53	37.5	3	-	6	-	537.7 ± 13.5 (0.105)	14.37 ± 1.52
6	53	37.5	3	0.5	3	-	581.0 ± 61.1 (0.201)	8.03 ± 0.70
7	53	25	3	0.5	3	-	507.0 ± 10.5 (0.099)	10.19 ± 0.69
8	53	37.5	3	0.75	3	-	579.6 ± 7.7 (0.115)	10.40 ± 1.14
9	53	37.5	4.5	0.5	3	-	548.6 ± 20.2 (0.130)	9.07 ± 2.45
10	53	37.5	6	0.5	3		984.9 ± 93.6 (0.103)	7.65 ± 0.85
11	53	37.5	6	-	-	10	553.5 ± 5.7 (0.196)	16.90 ± 4.13
12	53	37.5	6	-	-	16	488.4 ± 19.3 (0.213)	23.79 ± 1.81
13	53	50	6	-	-	10	469.6 ± 3.8 (0.202)	15.46 ± 2.32
14	53	100	6	-	-	10	624.3 ± 16.1 (0.205)	15.64 ± 3.12
15	53	37.5	4.5	0.5	-	10	462.7 ± 32.3 (0.227)	18.21 ± 1.67
16	53	37.5	6	0.5	-	10	476.4 ± 8.4 (0.196)	20.28 ± 1.10
17	53	50	6	0.5	-	10	374.5 ± 4.8 (0.232)	19.56 ± 1.73

Table 1

SLN	PTX EE%	PTX LOADING (µg PTX/mg BA)
0	78 ± 4	47 ± 2
1	85 ± 5	50 ± 3
2	89 ± 3	80 ± 3
3	90 ± 3	108 ± 4
4	70 ± 6	42 ± 4
5	25 ± 3	16 ± 2
6	87 ± 4	52 ± 2
7	98 ± 2	60 ± 1
8	65 ± 6	40 ± 4
9	92 ± 4	82 ± 3
11	77 ± 2	92 ± 2
12	81 ± 4	98 ± 5
13	52 ± 5	62 ± 6
14	24 ± 3	28 ± 3
15	83 ± 4	74 ± 3
16	83 ± 3	100 ± 4
17	75 ± 5	90 ± 6

889

890 Table 2

891

		SLN 9	SLN 15	SLN 16	SLN 17
7 days	Size (nm)	682.4 ± 15.1	783.2 ± 74.3	554.2 ± 9.5	500.1 ± 6.4
	%EE	92 ± 3	81 ± 2	80 ± 2	74 ± 3
	Zeta potential (mV)	9.15 ± 0.85	13.4 ± 0.9	15.9 ± 2.8	18.3 ± 1.6
30 days	Size (nm)	1500.0 ± 21.6	799.7 ± 63.2	598.1 ± 14.6	599.2 ± 9.5
	%EE	91 ± 4	80 ± 3	79 ± 3	73 ± 2
	Zeta potential (mV)	9.05 ± 0.54	11.6 ± 1.4	14.5 ± 3.3	14.4 ± 3.1
60 days	Size (nm)	1536.8 ± 39.2	933.8 ± 17.9	669.8 ± 27.3	686.1 ± 12.4
	%EE	89 ± 4	80 ± 3	71 ± 2	73 ± 2
	Zeta potential (mV)	9.07 ± 0.65	10.7 ± 2.1	13.9 ± 3.4	12.9 ± 4.1

892

893 Table 3

894

	SLN 9	SLN 15	SLN 16	SLN 17
Mean diameter (nm)	842.0 ± 17.9	632.4 ± 18.4	592.3 ± 18.0	408.4 ± 5.8
Zeta potential (mV)	8.66 ± 1.02	18.56 ± 1.34	19.68 ± 1.98	19.87 ± 1.45
PTX EE%	88 ± 3	81 ± 2	83 ± 2	89 ± 3

895 Table 4

896

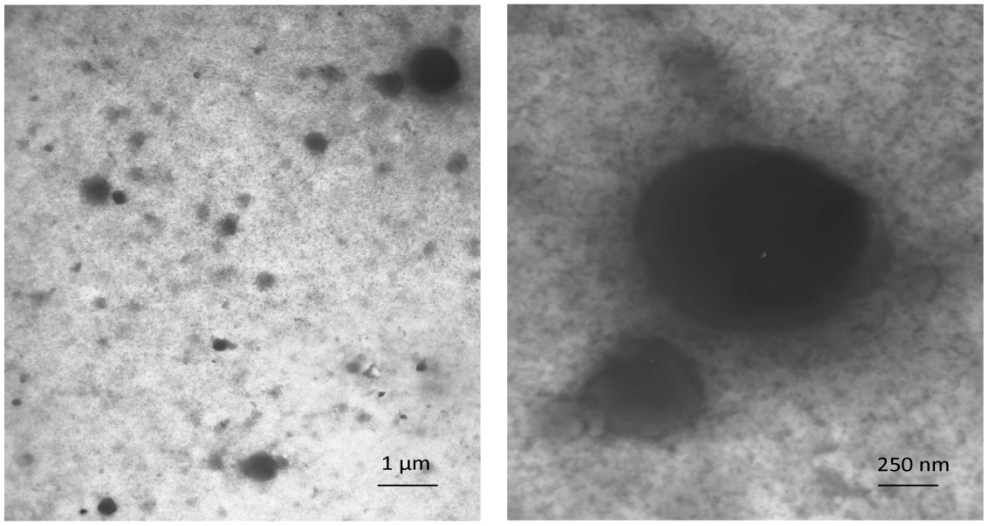

Figure 1a and 1b

Chirio et al

897

898

899

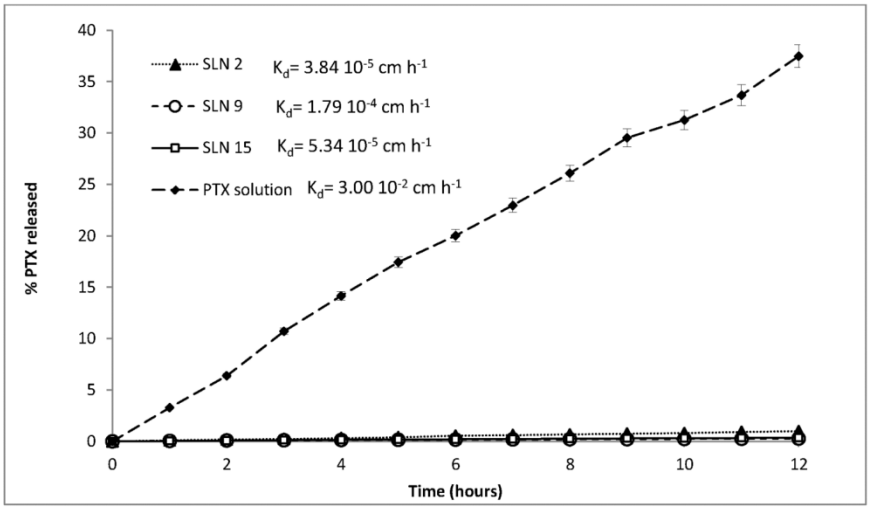

Figure 2

Chirio et al

900

901

902

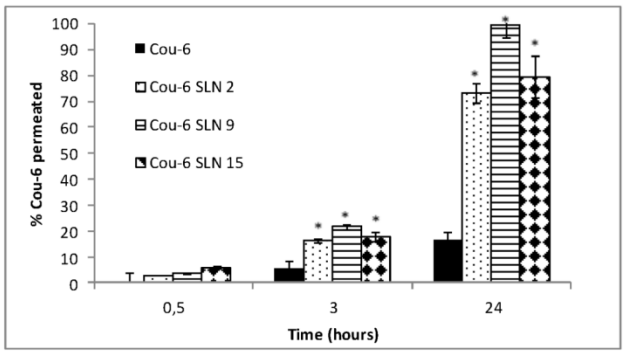

Figure 3

Chirio et al

903

904

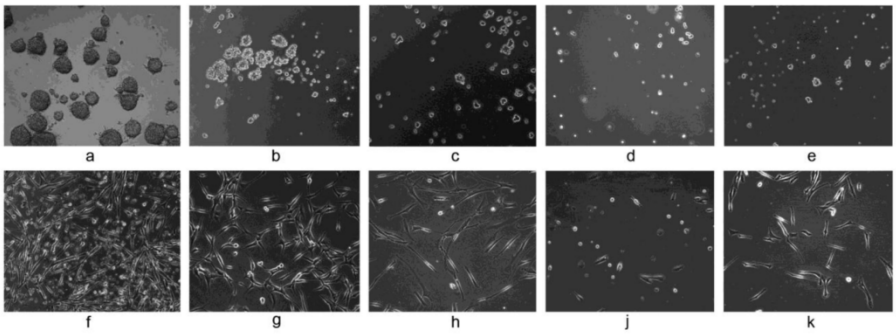

Figure 4

Chirio et al

905

906

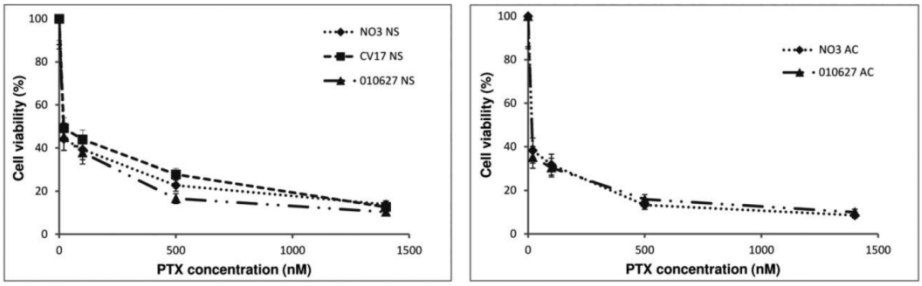

Figure 5

Chirio et al

907

908

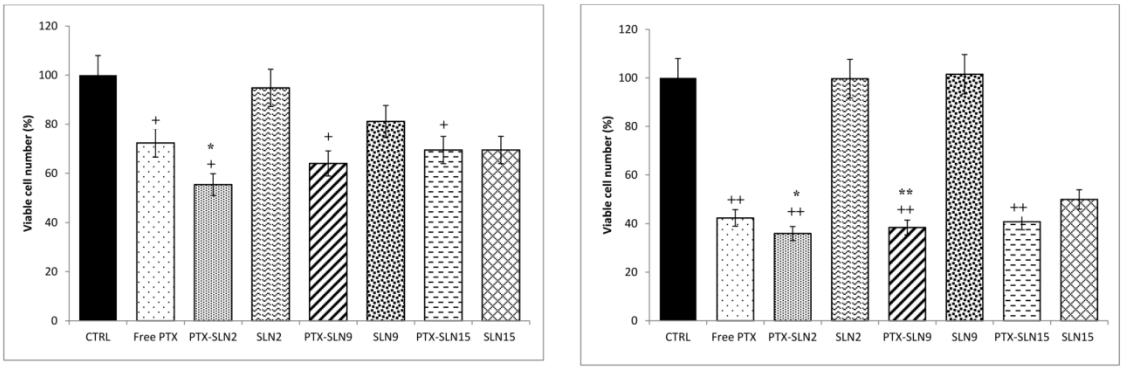

Figure 6

Chirio et al

909

910

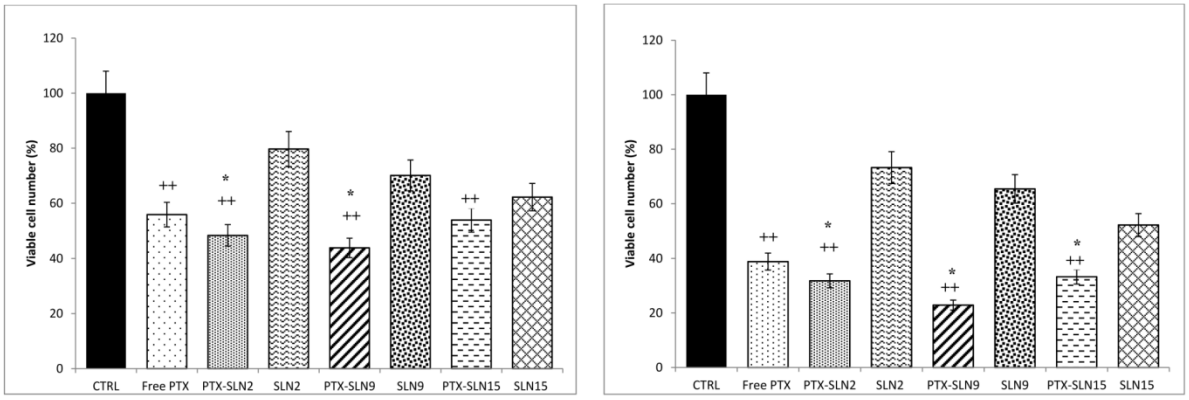

Figure 7

Chirio et al

911

912

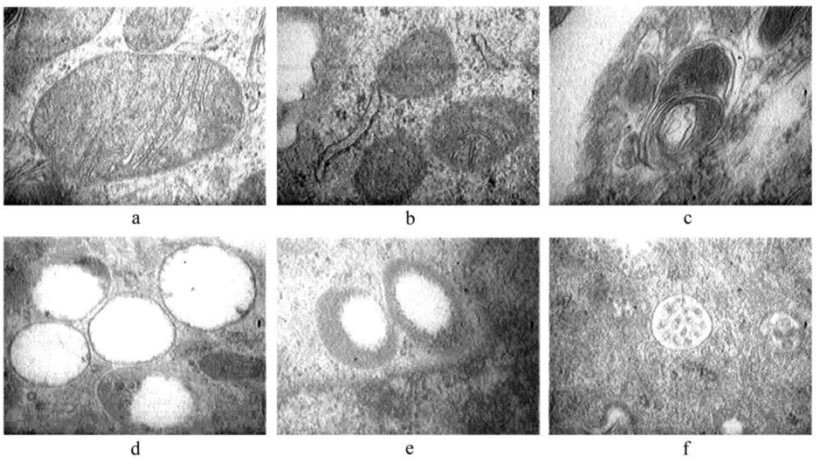

Figure 8

Chirio et al

913

914

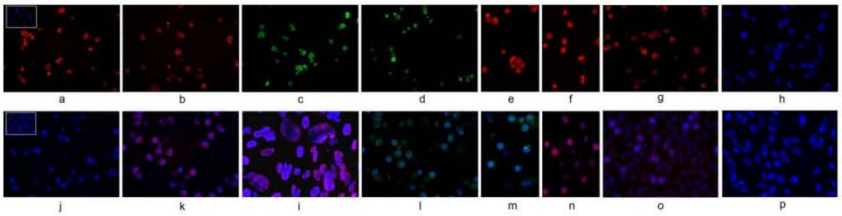

Figure 9

Chirio et al

915

916

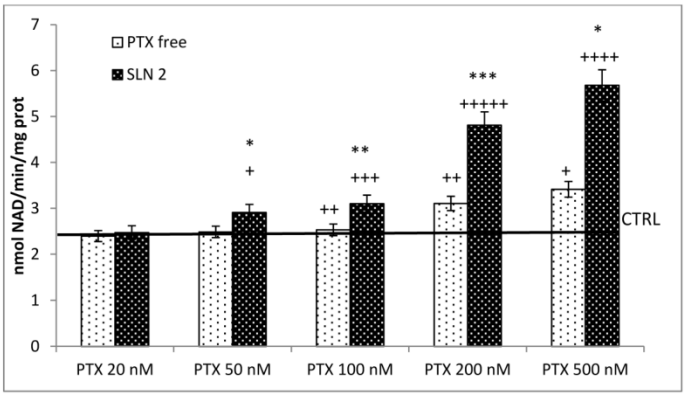

Figure 10

Chirio et al

917

918

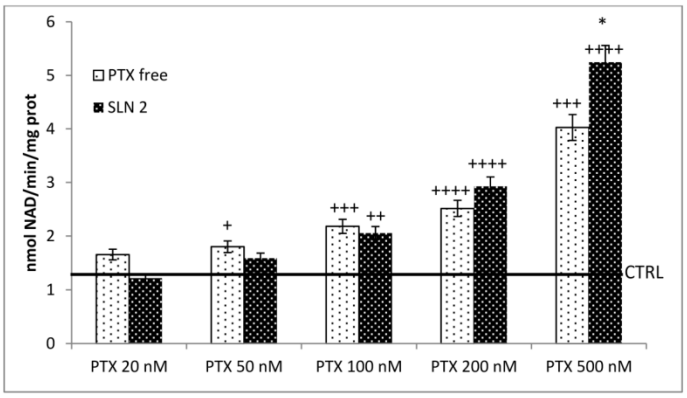

Figure 11

Chirio et al

919

920

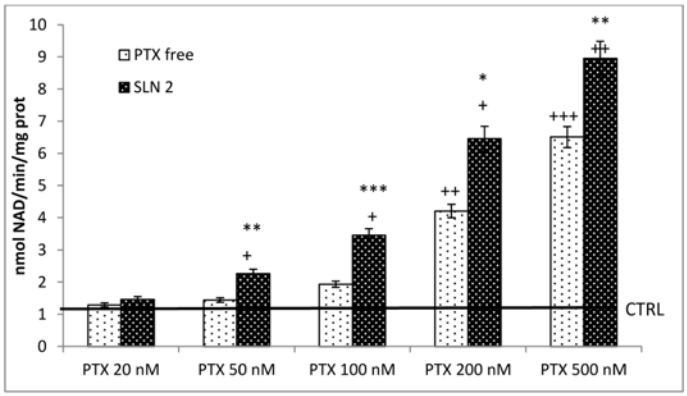

Figure 12

Chirio et al

921

922

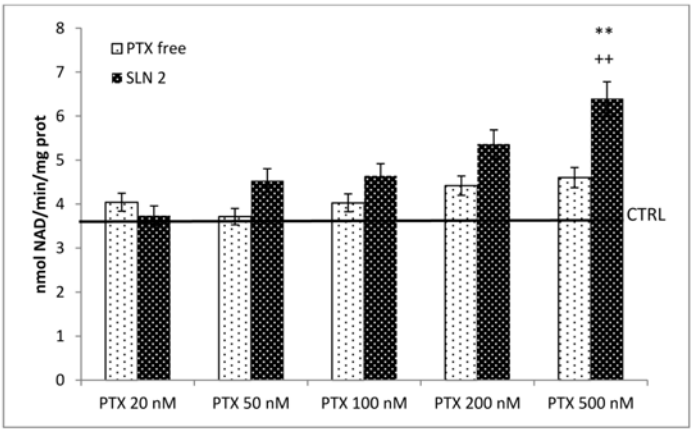

Figure 13

Chirio et al

923